Introduction to Modeling Thermoelectric Transport at High Temperatures

Andrew F. May[1] and G. Jeffrey Snyder[2]

[1]Materials Science and Technology Division, Oak Ridge National Lab., Oak Ridge, TN
[2]Materials Science, California Institute of Technology, Pasadena, CA

December 11, 2011

Contents

1 Introduction

The goal of this chapter is to provide experimentalists a basic outline for analyzing/modeling thermoelectric transport at high temperatures. The simplest model is that developed for itinerant conduction in a single parabolic band (SPB). The SPB model is a powerful analytical tool when investigating thermoelectric transport. For instance, it can be used to guide the enhancement and/or optimization of thermoelectric efficiency, or the analysis results may suggest the presence of more complex behavior affecting the thermoelectric efficiency. There are, of course, many cases when the SPB model fails due to either multi-band effects[1, 2] or non-parabolicity.[3, 4, 5, 6, 7] The interested reader has many texts available for studying the physical origin of thermoelectric transport and the models obtained from the Boltzmann transport equation.[8, 9, 10, 11, 12, 13, 14, 15]

A series of samples is not required to derive the parameters needed for a SPB model; indeed, it only takes data for a single sample. However, this modeling is best performed when a series of samples is available, as this allows the accuracy of the model to be tested. It is common for only a sample or two to be available, though, and in these cases the SPB model can suggest avenues to enhance the thermoelectric efficiency, such as increasing or decreasing the carrier density, and give a prediction for zT in an optimized sample.

1

Table 1: Summary of chemical potential dependence of a few pertinent properties for the case of acoustic phonon scattering. A table of Fermi integrals is provided in References [9, 14]. These tables are useful as a starting point in analysis, or to verify a computation is being performed correctly. The values of n are provided for $m^*/m_e = 1$ and $T = 300$ K.

η	α	L	n	r_H	$\frac{F_{-1/2}}{2F_0}$	ψ
(kT)	$(\mu\text{V K}^{-1})$	$(10^{-8}\,\text{W}\Omega\text{K}^{-2})$	(10^{19}cm^{-3})	(-)	(-)	$(\text{C K}^{-3/2}\,\text{m}^{-3})$
-3	433	1.49	0.123	1.17	0.877	28.3
-2	350	1.51	0.324	1.17	0.863	73.9
-1	272	1.54	0.823	1.16	0.832	182
0	205	1.61	1.92	1.13	0.773	403
1	151	1.72	3.95	1.11	0.693	764
2	112	1.86	7.09	1.08	0.610	1240
3	86.1	1.99	11.3	1.05	0.539	1770
4	68.2	2.09	16.3	1.04	0.482	2340
6	46.9	2.24	28.7	1.02	0.403	3490
8	35.4	2.32	43.6	1.01	0.351	4660
10	28.3	2.36	60.4	1.01	0.315	5820

Alternatively, a model developed for a novel compound may suggest that a large figure of merit zT is not achievable in the system without the introduction (or possibly the discovery) of irregular features in the transport properties. Thus, the SPB model is something of a diagnostic tool for both overall thermoelectric efficiency and the existence of more complex transport behavior.

It is essential to develop the SPB model in a region where minority carrier transport is negligible. A simple check for this is that the magnitude of the Seebeck coefficient α and electrical resistivity ρ are increasing with increasing temperature. This is typically the case in heavily doped (degenerate) semiconductors at moderate temperatures, before the thermal excitation of electron-hole pairs influences transport at higher temperatures. Such excitations are clearly revealed via a maximum in the magnitude of the temperature-dependent Seebeck coefficient and electrical resistivity, and often through a minimum in the thermal conductivity due to the onset of bipolar thermal conduction. The effective onset temperature depends on the carrier density, where a low carrier density promotes the influence of this bipolar conduction at lower temperatures. Therefore, it may be worthwhile to weight the data collected on a high carrier concentration sample more than that measured on a low carrier concentration sample.

The analysis and modeling of thermoelectric transport at high temperatures can be performed rather easily, particularly if in addition to the transport coefficients that make up the figure of merit ($zT = \alpha^2 T/\rho\kappa$), the Hall coefficient R_H is known. The Hall coefficient R_H provides a means to characterize a sample's carrier density ($n_H = 1/R_H e$) and mobility ($\mu_H = R_H/\rho$). When Hall data are not available, a rough estimate of the carrier density may be obtained via chemical considerations – the counting of formal valences or basic doping considerations. It is generally useful to compare a chemically-derived carrier density to one obtained via Hall measurements.[16]

1.1 Summary procedure for analyzing thermoelectric data with a single parabolic band model

The following simplified steps are utilized in the analysis and modeling of transport data at high temperatures via the single parabolic band (SPB) model. The equations presented in these steps assume a SPB with

conduction limited by acoustic phonon scattering. They employ the Fermi integrals F_j,

$$F_j(\eta) = \int_0^\infty f \epsilon^j \, d\epsilon = \int_0^\infty \frac{\epsilon^j \, d\epsilon}{1 + Exp[\epsilon - \eta]}. \tag{1}$$

Relevant example calculations are tabulated in Table 1 for comparison.

- This SPB model assumes acoustic phonon scattering limits the carrier mobility. Verify this by plotting $\log[\mu]$ versus $\log[T]$, which should give a slope between roughly -1 and -1.5. An acoustic phonon scattering assumption may be arguable for any slope $< $ -0.5.

- Obtain the SPB effective mass for a sample and temperature of interest. At a given T, calculate the reduced electrochemical potential η from the magnitude of the Seebeck coefficient (consider Table 1).

$$\alpha = \frac{k}{e} \left(\frac{2F_1}{F_0} - \eta \right) \tag{2}$$

Estimate m^* using η, the temperature and the carrier density (Table 1).

$$n = 4\pi \left(\frac{2m^* kT}{h^2} \right)^{3/2} F_{1/2} \tag{3}$$

The Hall carrier concentration ($n_H = 1/R_H e$) is related to the chemical carrier concentration n via $n_H = n/r_H$, where the Hall factor r_H for acoustic phonon scattering (see Table 1) is given by

$$r_H = \frac{3}{2} F_{1/2} \frac{F_{-1/2}}{2F_0^2}. \tag{4}$$

- Plot the magnitude of the Seebeck coefficient versus the Hall carrier density n_H at a given T (called by some a Pisarenko plot). Adjust the effective mass to obtain the best fit of the SPB model to the data for multiple samples, if available. This is the best stage to examine if the model is working well for the assumptions that m^* is independent of carrier concentration and multiple bands do not influence transport.

- Estimate the mobility parameter μ_0 at the temperature of interest. The Hall mobility $\mu_H = (\rho n_H e)^{-1}$ is typically used to estimate μ_0 from the SPB model. Non-degenerate (low carrier concentration and/or high T) semiconductors have $\mu_H = \frac{\sqrt{\pi}}{2} \mu_0$. The general SPB relationship utilizes μ_0 obtained from Equation 5 for μ_H (see Table 1), which assumes acoustic phonon scattering limits the carrier relaxation time. This equation can be used to explain the decrease in mobility with increasing carrier concentration at constant temperature using a plot similar to the Pisarenko plot for Seebeck coefficient.

$$\mu_H = \mu_0 \frac{F_{-1/2}}{2F_0} \tag{5}$$

If Hall data are not available at the temperature of interest, it may be reasonable to use the resistivity data with the assumption that the carrier concentration does not change with temperature.

- Calculate the Lorenz number L, using the following SPB equation or a plot of L versus α (Figure 5, Table 1).

3

$$L = \frac{k^2}{e^2} \frac{3F_0F_2 - 4F_1^2}{F_0^2} \tag{6}$$

Estimate the electronic contribution κ_e to the thermal conductivity. Subtract this from the total thermal conductivity and obtain an estimate for the lattice contribution κ_L,

$$\kappa_L = \kappa - \kappa_e = \kappa - L\sigma T. \tag{7}$$

If data for the phonon velocities are available (both the longitudinal v_l and transverse v_t velocities), compare the resultant κ_L to an estimation of κ_{min}. The following κ_{min} is developed by taking the high-temperature limit of the thermal conductivity calculated by Cahill *et al.*[17] for amorphous materials with an average volume per atom given by V.

$$\kappa_{min} = \frac{1}{2} \left(\frac{\pi}{6}\right)^{1/3} kV^{-2/3}(2v_t + v_l) \tag{8}$$

- Repeat these steps for other temperatures to obtain m^*, μ_0, and κ_L versus temperature, making sure the data do not demonstrate the influence of minority carrier transport.

- Calculate a theoretical zT versus n to estimate the optimum carrier density at a particular temperature. Using the parameters m^*, μ_0, and κ_L at a temperature of interest, calculate the β parameter.[18, 19, 20, 10]

$$\beta = \frac{\mu_0(m^*/m_e)^{3/2}T^{5/2}}{\kappa_L} \tag{9}$$

The function ψ also given in Table 1,

$$\psi = \frac{8\pi e}{3} \left(\frac{2m_e k}{h^2}\right)^{3/2} F_0, \tag{10}$$

is used to calculate the SBP prediction of zT from

$$zT = \frac{\alpha^2}{L + (\psi\beta)^{-1}}. \tag{11}$$

It is important to use the above method only for doping levels and temperatures where minority carrier effects would not be observed in the transport data. Thus, this method requires extrinsic samples and extrapolating within the extrinsic regime. In some circumstances, only an intrinsic sample is available; however, this can also be useful for assessing thermoelectric performance.

- The transport data of an intrinsic semiconductor may be utilized to estimate the thermal energy gap E_g and the lattice thermal conductivity κ_L.

The thermal band gap E_g is generally estimated in one of two ways. A traditional method is to plot ln[$1/\rho$] versus $1/T$, which should be linear with a *slope* = $-E_g/2k$. The second method [21] is to utilize the maximum in the magnitude of the Seebeck coefficient α_{max} and the corresponding temperature T_{max}, as shown in Equation 12. This estimate for E_g at high T is very useful in thermoelectrics,

as it quantifies the relative importance of minority carrier transport, which ultimately causes the decrease in zT at high temperature. It should also be noted that E_g can vary strongly with T, such as in PbTe.[3]

$$E_g = 2e\alpha_{max}T_{max} \qquad (12)$$

The value of κ_L can often be assumed equal to κ for an intrinsic semiconductor, particularly at moderate T. When κ of an intrinsic sample is decreasing with decreasing T, roughly as T^{-1}, it is reasonable to set $\kappa = \kappa_L$. However, if κ rises or appears to flatten at high T, then the bipolar thermal conductivity must also be considered.

2 Developing a single parabolic band model

Most high-performance thermoelectric materials are heavily-doped semiconductors with transport properties that appear more similar to metals than semiconductors. In general, electrical transport properties are determined by electrons (or holes) with energies near the electrochemical potential ζ, which is equal to the Fermi energy at $0\,\mathrm{K}$. In thermoelectric materials, the carrier density n tends to be independent of temperature, though some thermal activation of electron-hole pairs occurs at higher temperatures. For the most part, the transport properties observed at moderate/high temperatures are easily understood in terms of classical semiconductor physics. The electrical resistivity ($\rho = 1/\sigma = 1/ne\mu$) increases with increasing T as the carrier mobility μ decreases due to electron-phonon interactions. The magnitude of the Seebeck coefficient increases with increasing T as the reduced electrochemical potential $\eta = \zeta/kT$ decreases with increasing kT as well as the associated broadening of the Fermi distribution. A decrease in the carrier density also results in a reduced η (fixed T), and thus the Seebeck coefficient increases with decreasing carrier density.

The SPB model is expected to break down at the extremes of carrier density (and temperature). Non-parabolic or multi-band effects are more likely to be observed at higher carrier densities, when energies away from the band edge are probed. At low carrier densities, the deviation from the simple SPB model is more likely to be caused by a mobility edge, where a sharp decrease in μ may be observed due to carrier localization. Thermoelectric materials tend to optimize close by, but usually not in, the region where these features are significant.[9]

2.1 Hall mobility and carrier concentration

The carrier mobility provides insight into the nature of transport, and the temperature dependence of μ provides a strong indication of the dominant carrier scattering mechanism. To examine the theoretical temperature dependence of the Hall mobility μ_H, which is obtained via measurements of the Hall coefficient R_H and the electrical conductivity $\sigma = 1/\rho$, we consider the SPB model expression,

$$\mu_H = R_H\sigma = \frac{e}{m}\frac{\int_0^\infty \epsilon^{3/2}\tau^2\frac{\partial f}{\partial \epsilon}d\epsilon}{\int_0^\infty \epsilon^{3/2}\tau\frac{\partial f}{\partial \epsilon}d\epsilon}. \qquad (13)$$

The carrier mobility is closely related to the carrier relaxation time, τ, the value of which is generally obtained by inverse summation of the τ values associated with different scattering mechanisms. In semiclassical transport models, such as the SPB model, the τ for various scattering mechanisms are commonly modeled by power laws in reduced carrier energy $\epsilon = E/kT$: $\tau = \tau_0\epsilon^{\lambda-1/2}$. The parameter λ is often called the scattering parameter and assumes the value of 0 for scattering by acoustic phonons; $\lambda = 2$ is often

utilized for ionized impurity scattering. Note that in some representations λ may differ by the factor -1/2.[9] Assuming this simple power law for τ, integration by parts reduces Equation 13 to

$$\mu_H = \mu_0 \frac{(1/2 + 2\lambda)F_{2\lambda-1/2}}{(1 + \lambda)F_\lambda},$$ (14)

where $\mu_0 = e\tau_0/m^*$. Recall that F_j are dependent on η, which changes with T and thus the integrals F_j provide a temperature dependence in the various transport properties. The term μ_0 is used in the model that allows the optimum carrier density to be predicted for a given temperature. To calculate μ_0 from Equation 5 using experimental transport data, one must compute η, and this is typically achieved using the Seebeck coefficient. In other formulations, such as that given by Goldsmid,[9] expressions equivalent to Equation 5 are normalized so that μ_0 represents the non-degenerate mobility, or highest achievable mobility (when $\lambda = 0$) at the given T. The current definition for μ_0 utilizes the effective mass m^*, though it is more accurately defined as an inertial mass[13, 10] which is separate from the commonly called 'density of states effective mass' that is related to the carrier density (they are equal for the isotropic SPB). Note that the Hall mobility differs slights from the drift mobility, and the Hall factor r_H can be utilized to account for the minor difference (discussed below).

The temperature dependence of μ in a SPB arises due to two primary contributions (we consider only one relevant scattering mechanism). The first contribution is a power law in temperature introduced via the μ_0 term (more directly an associated τ_0). The second contribution is due to the η dependence of μ, which is hidden within the Fermi integrals; this introduces a temperature dependence because η changes with T and thus the necessary integrals are functions of T. Power laws in T can often be utilized to model both the μ_0 term and a ratio of Fermi-integrals.[14] Therefore, when a single scattering mechanism limits μ, the mobility often trends as roughly T^{-p} with an exponent $-p$ that may differ from the T-dependence observed (predicted) for μ_0. As such, a plot of $\log[\mu]$ versus $\log[T]$ can be informative when assessing the dominant scattering mechanism.

When acoustic phonon scattering limits τ, the deformation potential theory (for SPB) provides $\tau = \tau_{0,ac}\epsilon^{-1/2}$. The $\tau_{0,ac}$ is given by

$$\tau_{0,ac} = \frac{\pi\hbar^4 v_l^2 d}{\sqrt{2}E_{def}^2(m^*kT)^{3/2}},$$ (15)

where E_{def} is the deformation potential that relates to changes in the electronic structure due to the presence of a phonon.[14] This theory predicts that the mobility decreases with increasing T as T^{-p} where $1 \leq p \leq 1.5$. The limit $p = 1.5$ is obtained in a non-degenerate electron gas (low doping levels and/or high T) and originates in the τ_0 term; the $p = 1$ case is observed for highly-degenerate samples because $F_{-1/2}/F_0$ in Equation 5 goes as $\sim T^{0.5}$ for large η (the degenerate limit). A nice transition between the degenerate (metallic) $p = 1$ and semiconducting $p = 1.5$ is observed in $La_{3-x}Te_4$.[22]

It is important to note that significant deviations from this prediction are observed when material properties are temperature dependent. Considering Equation 15, it is clear that a temperature-dependent speed of sound (elastic properties), effective mass, or deformation potential can dramatically alter the temperature dependence of μ. For instance, a temperature-dependent m^* likely causes $\mu \propto T^{-2.5}$ in PbTe.[3] This is also observed in n-type $Ba_8Ga_{16-x}Ge_{30+x}$, as shown in Figure 1a, where the decay is closer to $T^{-1.9}$ at high temperatures. Generally, the observation of μ_H decreasing rapidly with increasing T suggests acoustic phonon scattering limits μ, and the model development can proceed.

The influence of additional scattering mechanisms may also be observed in the plot of $\log[\mu]$ versus $\log[T]$. For instance, a high residual resistance (from defects such as grain boundaries) reduces the overall p-value, as would scattering by ionized impurities ($\tau_0 \propto T^{3/2}$) and alloy scattering or optical phonon scattering
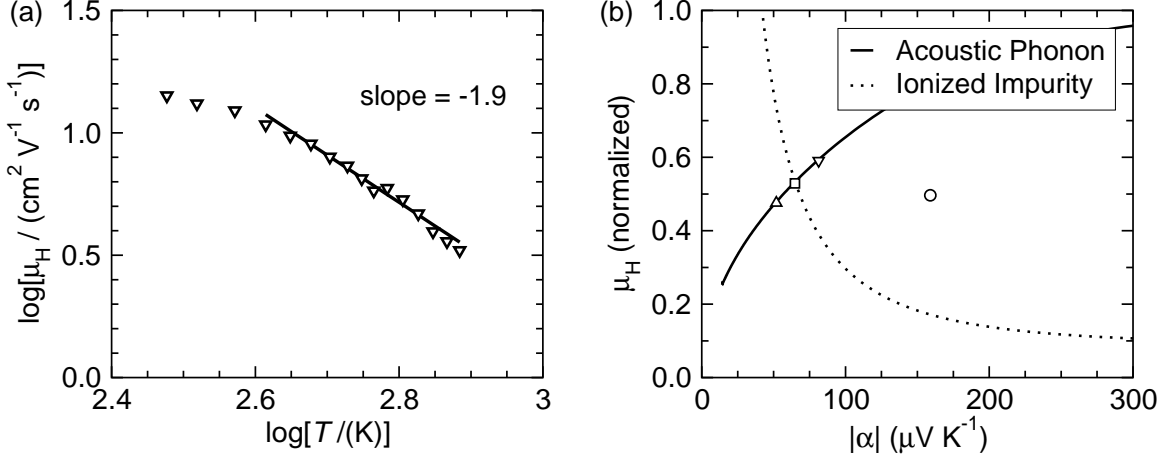
Figure 1: Hall mobility in n-type $Ba_8Ga_{16-x}Ge_{30+x}$, with experimental data shown by markers. (a) A generic power-law fit reveals that the mobility decays as roughly $T^{-1.9}$ at high temperatures. This behavior can be explained by acoustic phonon scattering when the effective mass increases with increasing T, as in PbTe.[3](b) The Hall mobility versus Seebeck coefficient can be utilized to probe the dominant scattering mechanisms, as shown here at 300 K; the sample with the highest Seebeck coefficient (the lowest carrier density) shows a deviation from the simple theory for acoustic phonon scattering, suggesting other scattering mechanisms are active in this sample. Note this simple model for ionized impurity scattering utilizes $\lambda = 2$ and a constant μ_0.

($\tau_0 \propto T^{-0.5}$). Indeed, in Figure 1a a lower p-value can be inferred from the data near room temperature, and it has been suggested that alloy scattering may be important in n-type $Ba_8Ga_{16-x}Ge_{30+x}$.[23] However, due to their respective T dependences, these scattering mechanisms tend to be less influential at high T where they lead to long relaxation times.

The energy-dependent portion of Equation 13 allows plots of μ_H versus n_H, or μ_H versus α to be examined. Such plots can also be used to verify the assumption that acoustic phonon scattering limits τ, as shown in References [24, 25]. For instance, in Figure 1b, three of the four n-type $Ba_8Ga_{16-x}Ge_{30+x}$ samples follow the behavior predicted for acoustic phonon scattering, while one sample deviates from the theoretical curve with no clear explanation. Note, these plots require several samples to be present, as the plot only makes physical sense at a given temperature.

To plot a theoretical n dependence, the carrier's SPB effective mass m^* must be known. It is common to obtain this using the experimental Hall carrier density n_H and the η obtained from α at a given T. However, the Hall carrier density ($n_H = 1/R_H/e$) is not exactly equal to the chemical carrier density (n in Equation 3). For parabolic bands, the two are equal when the electron gas is highly degenerate – this happens at low T and high n (large η, regardless of λ). In the limit of a non-degenerate electron gas, the chemical n is roughly 18% larger than n_H for the scattering of carriers by acoustic phonons ($\lambda = 0$). A self-consistent model calculates a theoretical Hall coefficient R_H to obtain $n_H = 1/R_H/e$, or employs the Hall factor $r_H = n/n_H = \mu_H/\mu$ to account for the difference. The error in using the chemical n is not extremely large, though, especially considering the primary goals of this analysis (estimating the optimal carrier density and assessing the electronic structure).

$$R_H = \frac{3h^3}{8\pi e(2m^*kT)^{3/2}} \frac{\int_0^\infty \epsilon^{3/2}\tau^2\frac{\partial f}{\partial \epsilon}d\epsilon}{(\int_0^\infty \epsilon^{3/2}\tau\frac{\partial f}{\partial \epsilon}d\epsilon)^2} \tag{16}$$

7
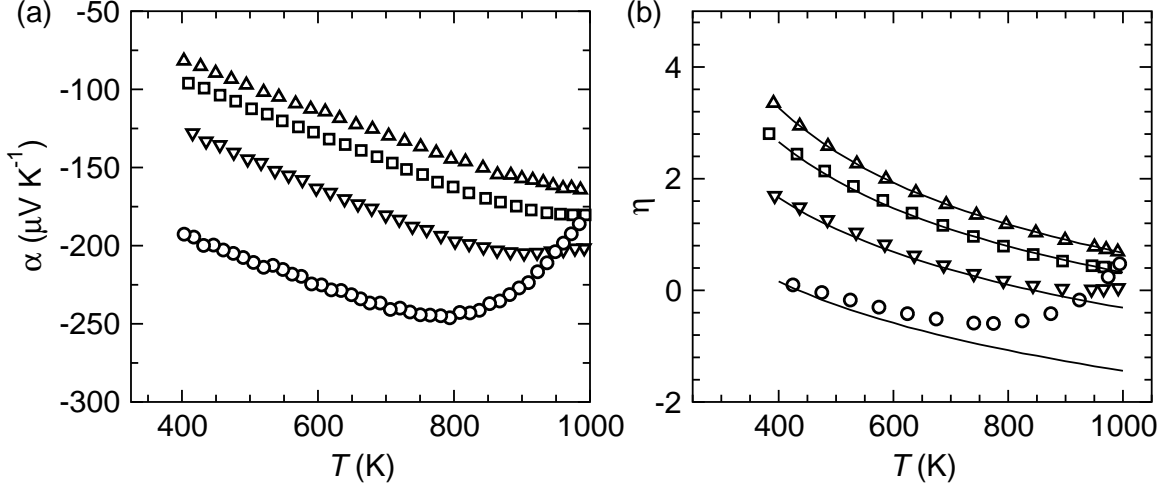
Figure 2: The temperature-dependent (a) Seebeck coefficient of n-type $Ba_8Ga_{16-x}Ge_{30+x}$ and the (b) reduced electrochemical potential η extracted from the data in (a) assuming a SPB model with electrons scattered by acoustic phonons. The result agrees well with the decay of η expected in a SPB with constant carrier density and band mass (solid curves). This is not true for the sample with the lowest carrier concentration, where the activation of minority carriers leads to a compensation of the Seebeck coefficient, and the rise of η at high T is an artifact of the SPB analysis. The carrier density of each sample can be inferred from Figure 3a where the symbols match.

For the simple power law description of the relaxation time $\tau = \tau_0 \epsilon^{\lambda - 1/2}$, this reduces to

$$R_H = \frac{3h^3}{8\pi e (2m^* kT)^{3/2}} \frac{(1/2 + 2\lambda) F_{2\lambda - 1/2}}{(1 + \lambda)^2 F_\lambda^2}. \tag{17}$$

The Hall factor r_H is then

$$r_H = \frac{3}{2} F_{1/2} \frac{(1/2 + 2\lambda) F_{2\lambda - 1/2}}{(1 + \lambda)^2 F_\lambda^2}. \tag{18}$$

2.2 The Seebeck coefficient

When developing a SPB model, one must verify that the minority carriers are not influencing the transport properties. An easy check for this is to examine the temperature dependence of the Seebeck coefficient. The Seebeck coefficient increases with increasing temperature and/or decreasing carrier density in a simple, extrinsically-doped semiconductor (n independent of T), because this T and/or n behavior corresponds to decreasing η. At high temperatures, the thermal activation of electron-hole pairs results in a compensation of the Seebeck coefficient, and a maximum in $|\alpha|$ is observed. Low extrinsic carrier concentrations promote the activation of electron-hole pairs due to lower η and a relative change in the charge neutrality equation. Clearly, the SPB model is not valid at the temperatures and compositions where the influence of minority carrier transport is observed, and theoretical predictions for transport at low carrier concentrations should be considered carefully.

The Seebeck coefficient behavior typically observed in heavily doped semiconductors is shown in Figure 2a, where experimental Seebeck coefficients are plotted versus T for n-type $Ba_8Ga_{16-x}Ge_{30+x}$.[25] The magnitude of α increases linearly with T at low/moderate T, then begins to lose linearity as the degeneracy

of the electron gas decreases. In the sample with the largest room temperature $|\alpha|$ (the lowest carrier density), the expected maximum in $|\alpha|$ is observed at high temperatures where holes influence transport. A similar maximum is observed in the corresponding resistivity data, and the thermal conductivity data also suggests bipolar conduction is important.[25] The E_g estimated via Equation 12 from the data in Figure 3a is $E_g = 0.4\,\text{eV}$, which is rather close to that obtained from resistivity data on a near-insulating sample.[25]

To analyze the Seebeck coefficient data, we utilize the SPB description:

$$\alpha = \frac{k}{e}\left(\frac{\int_0^\infty \epsilon^{3/2}(\epsilon - \eta)\tau \frac{\partial f}{\partial \epsilon}d\epsilon}{\int_0^\infty \epsilon^{3/2}\tau \frac{\partial f}{\partial \epsilon}d\epsilon}\right), \tag{19}$$

which reduces to the following when $\tau = \tau_0 \epsilon^{\lambda - 1/2}$

$$\alpha = \frac{k}{e}\left(\frac{(2+\lambda)F_{\lambda+1}}{(1+\lambda)F_\lambda} - \eta\right). \tag{20}$$

For a SPB, the Seebeck coefficient only depends on η. That is, regardless of the band mass, all parabolic bands have the same Seebeck coefficient at a given η (Table 1). A larger band mass results in a lower η for a given n, T, and thus larger m^* provides larger α for a given n due to lower η.

The value of η (relative to the band edge) can be estimated from experimental α data using Equation 2 (assumes $\lambda = 0$). This allows the (SPB) effective mass to be calculated from the expressions provided for n or n_H. An estimate of m^* can be obtained using the linear region of the $\alpha(T)$ curve and the degenerate-limit equation for α (Equation 22), which contains n and m^*.[26] This can be achieved without invoking a computational program, and is therefore appealing in some circumstances. However, such limiting expressions should be avoided when possible; the expressions containing integrals should be used to estimate the transport parameters and the predicted optimal carrier density and corresponding zT.

In the limit of a non-degenerate electron gas, where Boltzmann statistics apply, the Seebeck coefficient in a SPB is related to the carrier density n and effective mass m^* via

$$\alpha = \frac{k}{e}(2 + \lambda - \eta) = \frac{k}{e}\left(2 + \lambda + \ln\left[\frac{2\left(\frac{2\pi m^* kT}{h^2}\right)^{3/2}}{n}\right]\right). \tag{21}$$

While in the limit of a degenerate electron gas (large η, which is approximately equal to the Fermi energy E_F), the SPB description reduces to

$$\alpha = (1+\lambda)\frac{\pi^2 k^2 T}{3eE_F} = (1+\lambda)\frac{8\pi^2 k^2 T m^*}{3eh^2}\left(\frac{\pi}{3n}\right)^{2/3}. \tag{22}$$

The reduced electrochemical potential $\eta(T)$ obtained by analyzing $\alpha(T)$ in n-type $Ba_8Ga_{16-x}Ge_{30+x}$ is plotted in Figure 2b. The solid curves in Figure 2b are the theoretical dependence of η on T in a parabolic band, and have been obtained via Equation 3. These temperature-dependent, theoretical curves are generated by aligning the η values at 300 K via minor adjustments in m^* at a given n, or vice versa, and then changing T with constant n, m^* to obtain $\eta(T)$. The agreement between the theoretical curves and the data points obtained via $\alpha(T)$ is very good, and strongly suggests that the conduction band is parabolic for the n, T examined.

A region where the SPB model for n-type $Ba_8Ga_{16-x}Ge_{30+x}$ clearly fails is indicated by the rise in $\eta(T)$ at high temperatures for the sample with a maximum in $|\alpha(T)|$. The calculated value of η rises because the minority carrier contribution has not been taken into account. Indeed, the actual η is most likely still decreasing with increasing temperature. In a sample with a lower carrier density, the artificial rise in η
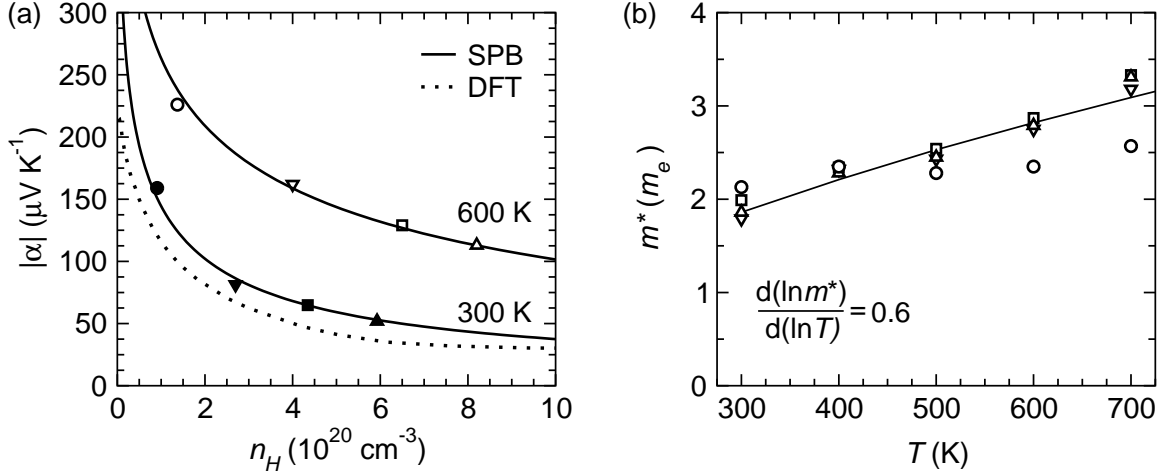
Figure 3: (a) The magnitude of the Seebeck coefficient in n-type $Ba_8Ga_{16-x}Ge_{30+x}$ is plotted versus the Hall carrier density and modeled by a SPB with m^*/m_e equal to 1.86 and 2.70 at 300 K and 600 K, respectively. Density functional theory calculation results[27] for 300 K are also shown, and the curvature agrees well with the SPB (DFT based results extracted from literature and plotted in n). (b) The effective masses obtained from the experimental Hall and Seebeck coefficients increase with increasing temperature in a manner similar to n-type PbTe. Symbols in (b) correspond to carrier concentration with same symbol in (a).

would occur at lower T, and thus the SPB model should not be utilized to consider low n data at high T. It is worth noting that a relatively simple two band model (identical band properties for holes and electrons) can capture the maximum in $|\alpha|$ and produce the expected $\eta(T)$, though it does not fully capture the observed n_H behavior. Developing an accurate two-band model is very difficult, as the energy gap and its temperature dependence, as well as the transport properties of minority carriers are often difficult to accurately address. For this reason, the two band model mentioned here is not shown, but is noted simply to encourage the reader to attempt more challenging models.

The plot of α versus n_H is one of the best tools to assess a material's *effective* band structure. This is achieved by calculating α versus η, and n_H versus η. The calculation of n or n_H versus η only needs to be performed once, and then the values of T and m^* can be changed appropriately to describe the data; as such, data for $m^*/m_e = 1$ and T=300 K are provided in Table 1. Once again, this reveals that n increases with increasing m^*, and that α is independent of band curvature for parabolic bands.

Similar to the comparisons shown in Figure 2b, agreement between the theoretical curves and the experimental data in Figure 3a strongly suggests conduction occurs in a single parabolic band for the n-type $Ba_8Ga_{16-x}Ge_{30+x}$ system. The experimental data are well described by a SPB model at both 300 K and 600 K (note that n_H increases slightly with T). Also shown on this plot is the result of a first principles calculation performed by Madsen and Singh,[27] which possesses similar curvature of $\alpha(n)$ at 300 K. Such a comparison to first principles calculations is often useful and may reveal interesting band features, as discussed below for $La_{3-x}Te_4$.

Interestingly, the SPB model suggests that the effective mass in $Ba_8Ga_{16-x}Ge_{30+x}$ increases with increasing temperature. The rise in m^* is similar to that observed in n-type PbTe, where $\Delta = \frac{d\ln m^*}{d\ln T} \sim 0.5$ is observed.[3] The increase in m^* is consistent with the strong temperature-dependence of the Hall mobility. However, Figure 2b demonstrates that constant n, m^* is consistent with the Seebeck coefficient data. The apparent increase in m^* is due to a gradual increase in n_H with increasing T.[25] Such behavior is
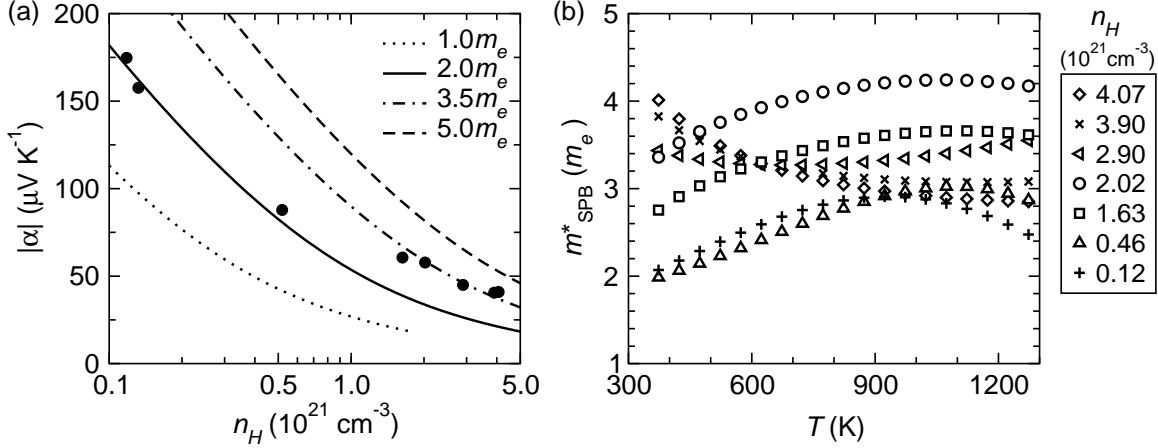
Figure 4: (a) In La$_{3-x}$Te$_4$, the carrier density dependence of $|\alpha|$ at 400 K suggests that multiple, parabolic bands contribute to the conduction process. The plot includes various band masses, which shift the calculated n_H to higher values with increasing m^*. (b) The single-band equivalent effective masses are heavily temperature dependent, and either increase or decrease with T, depending on the carrier concentration; this is another feature that suggests multiple bands contribute to conduction.

not expected in an extrinsic semiconductor, and thus the rise in m^* may be artificial. Therefore, despite the agreement between the data and the model, close inspection reveals that further investigation of the temperature-dependence of the band features is warranted.

In some cases, such as in La$_{3-x}$Te$_4$, the SPB model clearly fails to describe the available data. At first glance, the electrical transport in La$_{3-x}$Te$_4$ is as expected for a heavily-doped semiconductor, with the usual trends in α and σ being observed.[24] However, closer inspection of the Seebeck coefficient data reveals trends not consistent with conduction in a single parabolic band.[1] The influence of different carrier scattering mechanisms is important to consider here, as the defect concentration is very high. However, the dependence of μ on n and T is as expected for acoustic phonon scattering, and even the sample with the highest lanthanum vacancy concentration can be described by the simple theory presented above for acoustic phonon scattering.[24, 28]

The clearest example of how La$_{3-x}$Te$_4$ deviates from a SPB model is shown in Figure 4a, where the magnitude of α is plotted versus the room temperature Hall carrier density. Two different parabolic band models are required to describe the Seebeck coefficient data, though four are shown to illustrate the trends with effective mass more clearly. A large effective mass is necessary to describe $\alpha(n)$ at high carrier densities, while a smaller m^* is required at low carrier densities. This effect is most pronounced at low/moderate temperatures, because significant thermal broadening at high temperatures leads to a situation that is described fairly well by a SPB.

The calculated, 'SPB-equivalent' effective mass values are highly temperature dependent, and Figure 4b shows they do not trend with T in a simple manner. For the most part, this SPB effective mass of the electrons at high carrier concentrations decreases with increasing T, while that of the low carrier concentration samples increases with T. This irregular behavior is a very strong indication that transport occurs in multiple bands.

Given the above irregularities, it is desirable to perform first principles calculations to provide insight into how the electronic structure may be influencing transport. Density functional theory (DFT) calculations on La$_3$Te$_4$ confirmed[1] the existence of multiple conduction bands within the energy range of interest for
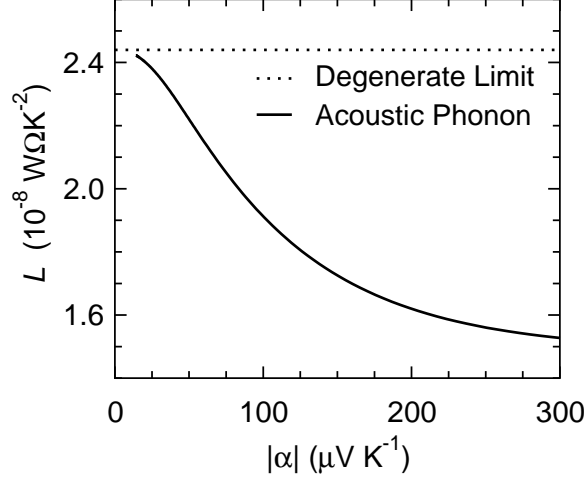
Figure 5: The Lorenz number expected in a SPB is plotted versus the Seebeck coefficient for acoustic phonon scattering (at all T). The dashed line represents the degenerate limit of L, which is rarely obtained in thermoelectric materials.

the given n, T values, and were thus an invaluable tool in understanding the transport in this system.

With the DFT results for band offsets and degeneracy as a starting point, a multi-parabolic band model can be pursued. Such a procedure allows a semi-empirical model guided by first principles to be developed, and thus a more reasonable model of the system results from an interplay between classical modeling and fundamental calculations.[1] The initial analysis of the data using the SPB model was a necessary first step, though, as it suggested that a more complex electronic structure was influencing the transport properties.

2.3 Thermal transport

The thermal conductivity κ is composed of two primary contributions, the electronic κ_e and the lattice κ_L. Reducing, or ideally eliminating, the lattice contribution is a primary goal of thermoelectric research, and thus determining κ_L is of great importance. It is customary to subtract an estimate for the electronic contribution from the measured κ and assume the remainder is the lattice contribution. Another method to determine κ_L is to plot κ versus σ (or σT) at a given temperature and obtain the value of κ_L from the intercept; this can only be done if transport data for a series of samples are available.

The electronic contribution is commonly calculated via the Wiedemann-Franz relationship, $\kappa_e = L\sigma T$, where L is the Lorenz number. While this method cannot account for electron-phonon interactions, it can provide a reasonable estimate for κ_L if an appropriate L is utilized. This method is only valid in the temperature range where minority carrier transport is negligible, or else the resulting κ_L may contain a fairly significant contribution from the bipolar thermal conductivity κ_b.

In the limit of a single parabolic band with $\tau \propto \epsilon^{\lambda-1/2}$ the Lorenz number is

$$L = \frac{k^2}{e^2} \frac{(1+\lambda)(3+\lambda)F_\lambda F_{\lambda+2} - (2+\lambda)^2 F_{\lambda+1}^2}{(1+\lambda)^2 F_\lambda^2}. \tag{23}$$

The Lorenz number depends on η and the energy dependence of τ, as is the case for α. As such, it can be plotted as a function of α for a given scattering mechanism. In doing this for acoustic phonon scattering, as shown in Figure 5, we see that the degenerate limit of L is not reached in good thermoelectric materials. This is another way of viewing that the degenerate limit expressions are, in general, approximate but not
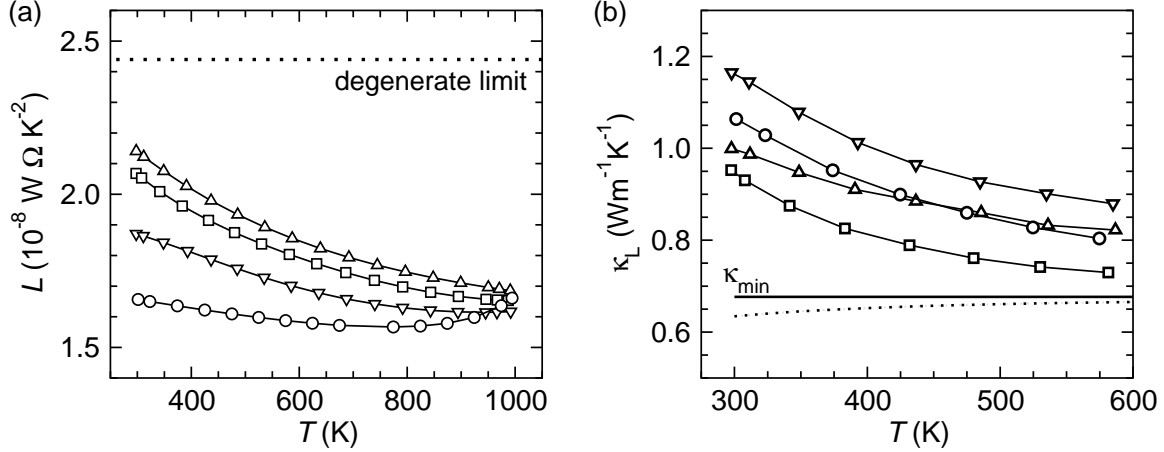
12

Figure 6: (a) The calculated Lorenz numbers for n-type $Ba_8Ga_{16-x}Ge_{30+x}$ [25] are consistently lower than the degenerate limit (dashed line), and at high temperatures the SPB fails as the L values increase artificially (because η rises artificially). (b) The lattice thermal conductivity is plotted in the temperature range where the bipolar contribution is negligible. This shows that κ_L approaches the minimum thermal conductivity at high temperatures, and thus introducing additional scattering mechanisms are only likely to reduce κ_L at moderate T. The solid lower curve shows represents κ_{min} in the high-temperature limit (Eqn. 8) and the dashed curve represents the more detailed calculation of κ_{min} (Eqn. 24).

accurate for thermoelectric materials. They do, however, provide insight into thermoelectric behavior and a decent starting point for understanding transport data.

The degenerate limit of the Lorenz number is given by $L = \pi^2 k^2/3/e^2 = 2.45 \times 10^{-8}$ WΩK^{-2}, and is valid at high degeneracy regardless of the carrier scattering mechanism. This limit is often utilized in transport analysis. At high temperatures, the use of this value typically results in an overestimation of L (κ_e) and thus an underestimation of κ_L. In such cases, attention is often drawn to the "low" value of κ_L and incorrect conclusions can be drawn regarding the physics governing thermoelectric efficiency and the best methods for increasing efficiency. Indeed, using the degenerate limit of L can even result in an apparently negative κ_L![24]

The results of SPB analysis of the thermal transport data for n-type $Ba_8Ga_{16-x}Ge_{30+x}$ are shown in Figure 6a,b for moderate temperatures. It is observed that the L values are significantly lower than the degenerate limit, as can be inferred from the magnitudes of α. At high temperatures, the SPB model breaks down where L is shown to artificially rise in the sample with the lowest carrier concentration. This is due to the compensation of the Seebeck coefficient and the corresponding rise (artificially) in η, which can be observed in Figure 2b. The calculated κ_L values are scattered about ~ 1 W/m/K at 300 K. The decrease in κ_L with increasing temperature is consistent with the *crystalline* behavior expected at high temperatures, where phonon-phonon interactions limit the phonon mean free path. As temperature rises and phonon populations increase linearly with T, phonon-phonon interactions increase and thus κ_L decreases as approximately T^{-1}. However, there is a minimum value for κ_L and thus the decay is not strictly at T^{-1}.[25] As with the carrier mobility, additional scattering mechanisms can also result in a reduced temperature dependence in κ_L, as is often observed in alloys or amorphous materials.

It can be very useful to compare the calculated κ_L to an estimate for the minimum κ_L, termed κ_{min} here. In doing so, we find that $Ba_8Ga_{16-x}Ge_{30+x}$ approaches this lower limit at high T, and thus phonon-phonon scattering produces very low κ in this material. The relatively low κ_L is also related to the large number of

13

atoms in the unit cell, which produces many optical phonons that generally have low group velocities.[29]

Cahill and Pohl provided a formula for the estimation of κ_{min} by considering transport in amorphous materials (Eqn. 24).[17] At high temperatures, this expression simplifies to Equation 8.

$$\kappa_{min} = \left(\frac{\pi}{6}\right)^{1/3} kV^{-2/3} \sum_i v_i \left(\frac{T}{\Theta_i}\right)^2 \int_0^{\Theta_i/T} \frac{x^3 e^x}{(e^x - 1)^2}\, dx \tag{24}$$

The summation is over the one longitudinal and two transverse modes, V represents the average volume per atom, $\Theta_i = v_i(\hbar/k_b)(6\pi^2/V)^{1/3}$, and v_i is the appropriate sound velocity.

The bipolar thermal conductivity arises due to the creation and annihilation of electron-hole pairs.[30] The bipolar thermal conductivity is related to the partial conductivities σ_i and Seebeck coefficients α_i of electrons (subscript n) and holes (subscript p),[31] and tends to rise rapidly at high temperatures due to the thermal activation of minority carriers. An unaccounted for κ_b often results in an apparent rise in κ_L at high T or a premature flattening to an apparent amorphous limit that is higher than expected.

$$\kappa_b = \frac{\sigma_p \sigma_n}{\sigma_p + \sigma_n}(\alpha_p - \alpha_n)^2 T \tag{25}$$

2.4 The optimization of zT

The net result of this process is a model for zT at moderate temperatures, where minority carriers do not significantly influence transport for the compositions of interest. As discussed above, the transport properties are strong functions of the reduced electrochemical potential η. The optimization process is thus an optimization in η, which is then correlated to an optimum carrier density n_{opt}. The optimum η occurs near the band edge (near $\eta = 0$), though its exact location depends on m^*, μ_0, and κ_L. Expressing zT as a function of energy-dependent terms α, L, and ψ allows the material-dependent terms to be grouped together in the factor β, shown in Equation 9.

It is important to note again that the SPB β hides the influence of band degeneracy in the effective mass m^*.[10] In this manner, this is truly an *effective* mass, as it averages out anisotropic effects, scattering influences, non-parabolicity, and the influence of multiple bands. When several bands are present, but have similar or identical energy minima, this method is particularly effective at providing a basic understanding of how zT optimizes as a function of n. A more accurate assessment of the band masses can be made by taking into account the presence of multiple bands, as discussed below regarding the number of equivalent valleys N_v.

For the case of any relaxation time that can be modeled by a simple power law in energy ($\tau = \tau_0 \epsilon^{\lambda - 1/2}$), the function ψ utilized in Equation 11 is given by

$$\psi = \frac{8\pi e}{3}\left(\frac{2 m_e k}{h^2}\right)^{3/2}(1 + \lambda)F_\lambda. \tag{26}$$

Enhancing zT can be seen as enhancing β, and it should be noted that a dependence on m^* is hidden within μ_0. In the limit of acoustic phonon scattering, the β factor is actually reduced when the effective mass increases, as μ_0 goes as $(m^*)^{-5/2}$ and thus the SPB zT decreases with increasing m^* for acoustic phonon scattering. Wood's review provides a nice discussion of the interplay between m^* and thermoelectric efficiency for various scattering mechanisms.[18]

For the n-type $Ba_8Ga_{16-x}Ge_{30+x}$ example, performing the zT versus n_H calculation at 600 K suggests an optimum composition near $n_H = 2 \times 10^{20} cm^{-3}$. This result is observed for models developed using data from two different carrier densities (solid and dashed curves), and a similar n_{opt} and maximum zT is
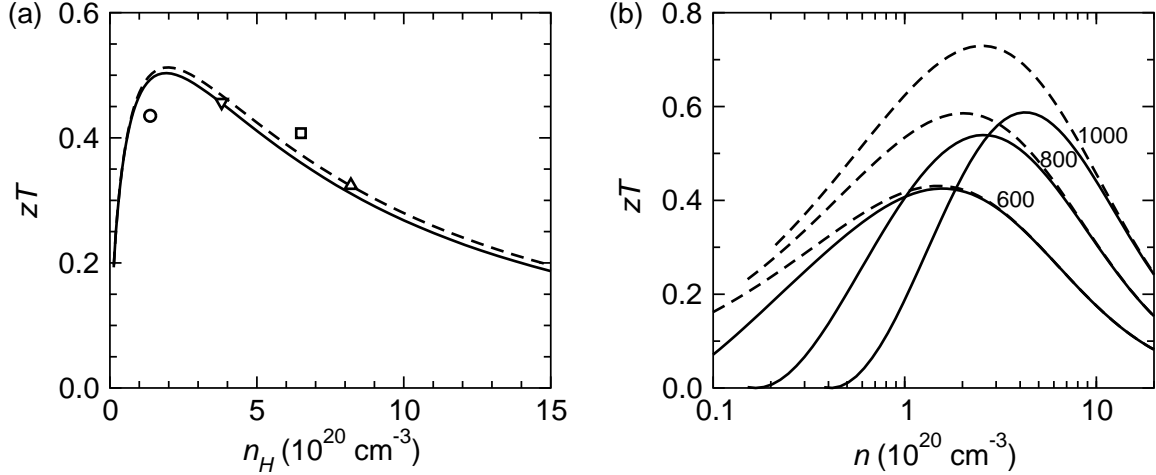
Figure 7: (a) The net result of the SPB is a theoretical zT versus n_H, shown here for $600\,\text{K}$ in n-type Ba$_8$Ga$_{16-x}$Ge$_{30+x}$, with an optimum composition predicted near $x = 0.25$ regardless of the input parameters; dashed and solid curves are generated by analyzing data for two different samples assuming $\lambda = 0$. (b) Theoretical zT versus n curves for a simple semiconductor show how n_{opt} increases with T. Also shown is the effect minority carriers can have on the maximum zT and the corresponding n_{opt} via a multi-carrier (2 band) model, which assumes similar μ_0 and m^* for electrons and holes. The dashed curves are the SPB models and the solid curves are for the two-band models, with temperatures indicated to the right of the curves. The parameters taken are similar to those in (a), but do not represent an accurate model for n-type Ba$_8$Ga$_{16-x}$Ge$_{30+x}$.

also obtained from a model developed assuming $\lambda = 0.5$.[25] While this model is likely to break down at much higher or lower n values, the region pertinent to thermoelectric application appears to be very well described, and thus the model achieves its primary task - to identify an optimum composition for application and identify means to enhance zT.

In many cases, only a single carrier density, or sample, is available. This is common in the exploration of novel compounds. It is useful to develop a basic model of transport to guide the optimization of performance. In some cases, this process indicates that large thermoelectric efficiency is unlikely to be achieved, and thus a simple model can save time in the exploration of novel compounds. The SPB model can also provide motivation to overcome synthetic difficulties. For instance, density functional theory calculations predicted n-type LiZnSb to have large thermoelectric efficiency.[32] While n-type samples have yet to be produced, the SPB model developed from two p-type samples suggested the assumptions utilized in the first principles calculations were reasonable, and thus the model provides further incentive to explore synthetic routes to obtain n-type LiZnSb.

Finally, Figure 7b shows a theoretical calculation of $zT(n)$ for a parabolic band(s) semiconductor. It is observed that n_{opt} increases with increasing T, and thus it is difficult to optimize a thermoelectric material over a wide temperature range. For simplicity, consider Ioffe's result obtained via power factor optimization in a non-degenerate electron gas, where $n_{opt} \sim (m^*T)^{3/2}$.[8] Even with this simplified approach to optimization, it is clear that *functionally graded materials* (with a spatially-dependent concentration of dopants) can provide significant enhancements in thermoelectric efficiency. See the chapter by E. Müller and G. J. Snyder in this text for further discussion on functionally graded materials.

Two sets of theoretical zT curves are plotted in Figure 7b. The dashed curves correspond to the SPB model shown in this chapter; the solid curves are for a simple semiconductor where electrons and holes

15

have identical m^* and μ_0, and E_g=0.4 eV. The effect of minority carriers is to reduce the overall zT due to compensation in α and the introduction of κ_b. To avoid the influence of these bipolar effects, the optimum carrier density shifts to higher values. For consistency with Figure 7a, the theoretical curves in Figure 7b are obtained using parameters similar to those for n-type $Ba_8Ga_{16-x}Ge_{30+x}$, but they do not represent an accurate model of transport in that system.

2.5   Expressions for multi-band conduction

The following equations are utilized to calculate the transport coefficients when multiple bands contribute to transport.[33] The calculation of transport parameters for each band i must take into account the energy scale of electrons in that band; the Fermi integrals can be modified to take into account the various band edge energies. Also, the Seebeck and Hall coefficients must possess their appropriate sign (negative for electrons and positive for holes).

The expression for the electronic contribution to the thermal conductivity (κ_e) contains two terms. The term on the left is a summation over the contribution from each band where the SPB L_i are utilized with the correct adjustments for relative energy scales; for a single band conductor this is the 'normal' electronic contribution. The term on the right exists due to transitions between different bands; in the limit that there is one electron band (n) and one hole band (p) this term reduces to the common expression for bipolar thermal conductivity (Equation 25).

$$n = \sum_i n_i \tag{27}$$

$$\sigma = \sum_i \sigma_i \tag{28}$$

$$R_H = \frac{\sum_i R_{H,i}\sigma_i^2}{(\sum_i \sigma_i)^2} \tag{29}$$

$$\alpha = \frac{\sum_i \alpha_i \sigma_i}{\sum_i \sigma_i} \tag{30}$$

$$\kappa_e = T(\sum_i L_i \sigma_i) + T\left(\sum_i \sigma_i \alpha_i^2 - \frac{(\sum_i \sigma_i \alpha_i)^2}{\sum_i \sigma_i}\right) \tag{31}$$

These expressions can be utilized to incorporate the influence of band degeneracy (multiple valleys with an equivalent energy minimum). In thermoelectrics, it is desirable to have a high band degeneracy,[10] as this promotes the simultaneous existence of large Seebeck and conductivity. The SPB model discussed here hides the influence of band degeneracy within the effective mass. If the band degeneracy is known, an estimate of m^* that is closer to the actual band mass can be obtained by incorporating this knowledge into the model. For N_v equivalent valleys, the SPB effective mass m^* is related to the density of states band mass m_{DOS} via $(m^*)^{3/2} = N_v(m_{DOS})^{3/2}$ (consider Equations 3 and 27).

3   Acknowledgements

4 List of Symbols

d	density
E	particle energy
e	magnitude of charge of an electron or hole
E_{def}	deformation potential
f	Fermi distribution function
F_j	Fermi integral of order j
h	Planck constant
k	Boltzmann constant
L	Lorenz number
m_e	rest mass of electron
m^*	carrier effective band mass
n	carrier density
n_H	Hall carrier density ($= 1/R_H e$)
n_{opt}	optimum carrier density
p	generic power law fit parameter for temperature-dependence of mobility
R_H	Hall coefficient
r_H	Hall factor
T	absolute temperature
V	average volume per atom
v_l	longitudinal speed of sound
v_t	transverse speed of sound
zT	thermoelectric figure of merit (materials, dimensionless)
α	Seebeck coefficient
ϵ	reduced particle energy ($= E/kT$)
ζ	electrochemical potential
η	reduced electrochemical potential ($= \zeta/kT$)
κ	thermal conductivity
κ_b	bipolar contribution to thermal conductivity
κ_e	electronic contribution to thermal conductivity
κ_L	lattice or phonon contribution to thermal conductivity
κ_{min}	minimum lattice thermal conductivity
λ	scattering parameter related to energy dependence τ
μ	drift mobility
μ_H	Hall mobility
μ_0	SPB mobility parameter ($= e\tau_0/m^*$)
ρ	electrical resistivity
σ	electrical conductivity
τ	relaxation time for a charge carrier
τ_0	prefactor in power law description of energy-dependent τ

References

[1] A. F. May, D. J. Singh, G. J. Snyder, Influence of band structure on the large thermoelectric performance of lanthanum telluride, *Physical Review B* **79**, 153101 (2009).

[2] D. J. Singh, I. I. Mazin, Calculated thermoelectric properties of La-filled skutterudites, *Physical Review B* **56**, R1650 (1997).

[3] Y. I. Ravich, B. A. Efimova, I. A. Smirnov, *Semiconducting Lead Chalcogenides* (Plenum, New York, 1970).

[4] D. J. Singh, W. E. Pickett, Skutterudite antimonides: Quasilinear bands and unusual transport, *Phys. Rev. B* **50**, 11235–11238 (1994).

[5] T. Caillat, A. Borshchevsky, J.-P. Fleurial, Properties of single crystalline semiconducting $CoSb_3$, *Journal of Applied Physics* **80**, 4442 (1996).

[6] J. S. Dyck, W. Chen, C. Uher, L. Chen, X. Tang, T. Hirai, Thermoelectric properties of the n-type filled skutterudite $Ba_{0.3}Co_4Sb_{12}$ doped with Ni, *Journal of Applied Physics* **91**, 3698 (2002).

[7] V. L. Kuznetsov, L. A. Kuznetsova, D. M. Rowe, Effect of partial void filling on the transport properties of $Nd_xDo_4Sb_{12}$ skutterudites, *Journal of Physics: Condensed Matter* **15**, 5035 (2003).

[8] A. F. Ioffe, *Semiconductor Thermoelements and Thermoelectric Cooling* (Infosearch Ltd, London, 1957).

[9] H. J. Goldsmid, *Applications of Thermoelectricity* (Butler & Tanner Ltd, London, 1960).

[10] H. J. Goldsmid, *Introduction to Thermoelectricity* (Springer, New York, 2009).

[11] A. H. Wilson, *The Theory of Metals* (The Syndics of the Cambridge University Press, London, 1953).

[12] J. M. Ziman, *Electrons and Phonons. The Theory of Transport Phenomena in Solids* (Oxford University Press, London, 1963).

[13] C. M. Bhandari, *CRC Handbook of Thermoelectrics* (CRC Press LLC, New York, 1995).

[14] V. I. Fistul, *Heavily Doped Semiconductors* (Plenum Press, New York, 1969).

[15] N. W. Ashcroft, N. D. Mermin, *Solid State Physics* (Thomson Learning Inc, United States of America, 1976).

[16] E. S. Toberer, A. F. May, G. J. Snyder, Zintl chemistry for designing high efficiency thermoelectric materials, *Chemistry of Materials* **22**, 624-634 (2010).

[17] D. G. Cahill, S. K. Watson, R. O. Pohl, Low limit to the thermal conductivity of disordered crystals, *Physical Review B* **46**, 6131-6140 (1992).

[18] C. Wood, Materials for thermoelectric energy conversion, *Reports on Progress in Physics* **51**, 459-539 (1988).

[19] G. D. Mahan, *Solid State Physics*, vol. 51 (Academic Press, New York, 1998).

[20] F. DiSalvo, Thermoelectric cooling and power generation, *Science* **285**, 703 (1988).

[21] H. J. Goldsmid, J. W. Sharp, Estimation of the thermal band gap of a semiconductor from Seebeck measurements, *Journal of Electronic Materials* **28**, 869-872 (1999).

[22] L. Danielson, M. Alexander, C. Vining, R. Lockwood, C. Wood, Thermoelectric properties of LaTe$_y$, *Proceedings Seventh International Conference on Thermoelectric Energy Conversion*, University of Texas, Arlington, Texas; p. 71 (March 1988).

[23] M. Hokazono, H. Anno, K. Matsubara, Effect of Cu substitution on thermoelectric properties of Ge clathrates, *Materials Transactions* **46**, 1485-1489 (2005).

[24] A. F. May, J.-P. Fleurial, G. J. Snyder, Thermoelectric performance of lanthanum telluride produced via mechanical alloying, *Physical Review B* **78**, 125205 (2008).

[25] A. F. May, E. S. Toberer, A. Saramat, G. J. Snyder, Characterization and analysis of thermoelectric transport in *n*-type Ba$_8$Ga$_{16-x}$Ge$_{30+x}$, *Physical Review B* **80**, 125205 (2009).

[26] E. S. Toberer, G. J. Snyder, Complex thermoelectric materials, *Nature Materials* **7**, 105-114 (2008).

[27] G. K. H. Madsen, K. Schwarz, P. Blaha, D. J. Singh, Electronic structure and transport in Type-I and Type-VIII clathrates containing strontium, barium, and europium, *Physical Review B* **68**, 125212 (2003).

[28] A. F. May, E. Flage-Larsen, G. J. Snyder, Electron and phonon scattering in the high temperature thermoelectric La$_3$Te$_{4-z}M_z$, M= Sb,Bi, *Physical Review B* **81**, 125205 (2010).

[29] M. Christensen, A. B. Abrahamsen, N. B. Christensen, F. Juranyi, N. H. Andersen, K. Lefmann, J. Andreasson, C. R. H. Bahl, B. B. Iversen, Avoided crossing of rattler modes in thermoelectric materials, *Nature Materials* **7**, 811-815 (2008).

[30] H. J. Goldsmid, The thermal conductivity of bismuth telluride, *Proceedings of the Physical Society B,* **69** 203 (1956).

[31] H. J. Goldsmid, *The Thermal Properties of Solids* (Dover Publications, New York, 1965).

[32] G. K. H. Madsen, Automated search for new thermoelectric materials: The case for LiZnSb, *Journal of the American Chemical Society* **128**, 12140-12146 (2006).

[33] E. H. Putley, Galvano- and thermo-magnetic coefficients for a multi-band conductor, *J. Phys. C: Solid State Phys.* **8**, 1837-1840 (1975).